

Dynamically tunable multiband plasmon-induced transparency effect based on graphene nanoribbon waveguide coupled with rectangle cavities system

Zi-Hao Zhu(朱子豪), Bo-Yun Wang(王波云), Xiang Yan(闫香), Yang Liu(刘洋), Qing-Dong Zeng(曾庆栋), Tao Wang(王涛), and Hua-Qing Yu(余华清)

Citation: Chin. Phys. B, 2022, 31 (**8**): 084210. DOI: 10.1088/1674-1056/ac7e39
Journal homepage: http://cpb.iphy.ac.cn; http://iopscience.iop.org/cpb

What follows is a list of articles you may be interested in

An ultrafast and low-power slow light tuning mechanism for compact aperture-coupled disk resonators

Bo-Yun Wang(王波云), Yue-Hong Zhu(朱月红), Jing Zhang(张静), Qing-Dong Zeng(曾庆栋), Jun Du(杜君), Tao Wang(王涛), Hua-Qing Yu(余华清)

Chin. Phys. B, 2020, 29 (**8**): 084211. DOI: 10.1088/1674-1056/ab9df1

Tunable plasmon-induced transparency based on asymmetric H-shaped graphene metamaterials

Yu-Chen Tian(田雨宸), Wei Jia(贾微), Pei-Wen Ren(任佩雯), Chun-Zhen Fan(范春珍)

Chin. Phys. B, 2018, 27 (**12**): 124205. DOI: 10.1088/1674-1056/27/12/124205

Broadrange tunable slow and fast light in quantum dot photonic crystal structure

Alireza Lotfian, Reza Yadipour, Hamed Baghban

Chin. Phys. B, 2017, 26 (**12**): 124207. DOI: 10.1088/1674-1056/26/12/124207

Coupled-resonator-induced transparency in two microspheres as the element of angular velocity sensing

Kun Qian(钱坤), Jun Tang(唐军), Hao Guo(郭浩), Wei Zhang(张伟), Jian-Hua Liu(刘建华), Jun Liu(刘俊), Chen-Yang Xue(薛晨阳), Wen-Dong Zhang(张文栋)

Chin. Phys. B, 2016, 25 (**11**): 114209. DOI: 10.1088/1674-1056/25/11/114209

Role of incoherent pumping and Er^{3+} ion concentration on subluminal and superluminal light propagation in Er^{3+}-doped YAG crystal

Seyyed Hossein Asadpour, H. Rahimpour Soleimani

Chin. Phys. B, 2015, 24 (**1**): 014204. DOI: 10.1088/1674-1056/24/1/014204

Dynamically tunable multiband plasmon-induced transparency effect based on graphene nanoribbon waveguide coupled with rectangle cavities system

Zi-Hao Zhu(朱子豪)[1,†], Bo-Yun Wang(王波云)[1,2,†,‡], Xiang Yan(闫香)[1], Yang Liu(刘洋)[1], Qing-Dong Zeng(曾庆栋)[1], Tao Wang(王涛)[2], and Hua-Qing Yu(余华清)[1]

[1] *School of Physics and Electronic-information Engineering, Hubei Engineering University, Xiaogan* 432000, *China*
[2] *Wuhan National Laboratory for Optoelectronics, Huazhong University of Science and Technology, Wuhan* 430074, *China*

(Received 11 May 2022; revised manuscript received 1 July 2022; accepted manuscript online 5 July 2022)

A dynamically tunable multiband plasmon-induced transparency (PIT) effect in a series of rectangle cavities coupled with a graphene nanoribbon waveguide system is investigated theoretically and numerically by tuning the Fermi level of the graphene rectangle cavity. A single-PIT effect is realized using two different methods: one is the direct destructive interference between bright and dark modes, and the other is the indirect coupling through a graphene nanoribbon waveguide. Moreover, dual-PIT effect is obtained by three rectangle cavities side-coupled with a graphene nanoribbon waveguide. Results show that the magnitude of the dual-PIT window can be controlled between 0.21 and 0.74, and the corresponding group index is controlled between 143.2 and 108.6. Furthermore, the triple-PIT effect is achieved by the combination of bright–dark mode coupling and the cavities side-coupled with waveguide mechanism. Thus, sharp PIT windows can be formed, a high transmission is maintained between 0.51 and 0.74, and the corresponding group index is controlled between 161.4 and 115.8. Compared with previously proposed graphene-based PIT effects, the size of the introduced structure is less than 0.5 μm^2. Particularly, the slow light effect is crucial in the current research. Therefore, a novel approach is introduced toward the realization of optical sensors, optical filters, and slow light and light storage devices with ultra-compact, multiband, and dynamic tunable.

Keywords: plasmon-induced transparency (PIT), graphene, group index, rectangle cavities

PACS: 42.25.Bs, 81.05.ue, 47.11.Bc **DOI:** 10.1088/1674-1056/ac7e39

1. Introduction

Electromagnetically induced transparency (EIT) effect,[1,2] a quantum effect, which is caused by the destructive interference between the two different pathways excited in the so-called three-level atomic systems,[2] has shown various potential applications in fields, such as slowing light,[3,4] light storage,[5] and optical filtering.[6] However, effective nonlinear materials and rigorous conditions are difficult to be achieved, thereby significantly limiting the integrated application in practical optical devices. However, the plasmon-induced transparency (PIT) effect obtained by the cavity coupled with a plasmonic waveguide systems has caused extensive attention on account of simple realization. The devices realizing the PIT effect can be fabricated with a small footprint because surface plasmon polaritons (SPPs) can support deep subwavelength scale modes and overcome classical diffraction limit.[7–9] At present, diversified structures of PIT effect realization have been proposed. Moreover, the cavities side-coupled with a waveguide and the bright-dark mode coupling methods are of special guidance for generating a PIT window in various structures;[10–13] these methods are beneficial to on-chip integration plasmonic devices, thereby facilitating easy fabrication of an ultra-compact structure.

Thus far, many plasmonic devices for realizing PIT effect have been investigated, and the cavities coupled with a metal-dielectric-metal (MDM) plasmonic waveguide is particularly prominent in highly integrated devices. Moreover, the coupling of MDM waveguides with double U-cavity,[14] double-stub cavities,[15] and double-disk cavities[16] have a great deal of research in the area of integrated slow light devices. However, only structural parameters can be adjusted once the devices are designed. Thus, obtaining dynamically tunable PIT effects at a specific wavelength is difficult. Graphene, a novel two-dimensional (2D) material for tunable optical devices, comprises a single layer of carbon atoms; it has been recently widely considered by researchers due to its advantages of dynamic tunability, strong locality, and low loss.[17] The Fermi level of graphene can be flexibly controlled by applying varying applied voltage. Therefore, this feature provides graphene with an advantage for new tunable photonic device materials. Thus, many PIT devices made of graphene with excellent slow light properties and dynamic tunability, such as plasmonic waveguide coupled with nanocavities,[18,19] metamaterials,[20–23] and metallic grating coupled with a di-

[†] These authors contributed equally to this work.
[‡] Corresponding author. E-mail: wangboyun@alumni.hust.edu.cn

© 2022 Chinese Physical Society and IOP Publishing Ltd

electric waveguide layer (GCDWL) structures, have been proposed due to these unique performance advantages. Among of the various graphene structures, fabricating metamaterials and GCDWL structures through the current fabrication process is relatively complicated on accountof the limitation of the micro machining etching accuracy.[24] Furthermore, integrating metamaterials and GCDWL structures into the plasmonic chip is complicated.[25,26]

Compared with complicated metamaterials and GCDWL structures, the graphene nanoribbon waveguide structure has obtained widespread attention and achievements because of its easy integration, ultranarrow bandwidth, high transmission, and relatively simple fabrication.[27–29] For instance, Lu *et al.* have numerically and theoretically investigated the plasmonic resonant effect and propagation characteristics by changing physical parameters such as the chemical potential and width of the graphene nanoribbon in a nanoscale graphene waveguide system consisting of a monolayer graphene nanoribbon coupled with two guided-wave graphene sheets, which provide a new way toward the realization of nanoscale mid-infrared spectral control and graphene plasmonic devices.[30] A dynamic tunable PIT effect is achieved in our structures inspired by this research. Wang *et al.* proposed tunable PIT effect based on Fabry–Perot resonance in a system by using two rectangle graphene cavities coupled with a graphene nanoribbon waveguide, which causes a relatively wide transmission window.[31] Noual *et al.* designed a compact graphene-based waveguide coupled to two rectangular cavity structures comprising graphene nanoribbons. In addition, the peak of the PIT window is less than 0.6 in this structure.[32] Zhao *et al.* reported that graphene nanoribbon systems comprise a graphene strip loaded with a complex structure of graphene stub and ring cavity, thereby obtaining a considerably sharp PIT window. However, only a single-band PIT effect is acquired in the system.[33] Therefore, a dynamic tunable multiband PIT effect realized by graphene nanoribbon waveguide structure in the THz band remains relatively challenging.

For the fabrication of the graphene nanoribbon waveguide, it should be noticed that lithographic patterning lacks atomic resolution, which causes a mixture of armchair edges, zigzag edges, and dangling bonds; results in high line-edge roughness; and functionalizes the graphene nanoribbon edges.[34] Such inhomogeneities and disorder lead to severely degraded carrier mobility and thermal conductivity, coulomb blockade, and high off-currents-with effects that become increasingly detrimental with decreasing the graphene nanoribbon width.[34] Due to the fabrication defects of graphene resonators and nanoribbon waveguides, radiation loss and so on, the measured Q value and group index are usually much smaller in real experiments. Obviously, it is necessary to control the defects formation and the width edge roughness of the graphene nanoribbons in the nano-patterning process. Therefore, some important progresses have been reported. Wang *et al.* devised a gas phase chemical approach to etch graphene from the edges without damaging its basal plane. The reaction involved high temperature oxidation of graphene in a slightly reducing environment in the presence of ammonia to afford controlled etch rate ($\leq$ 1 nm/min). 20 nm–30 nm wide graphene nanoribbon waveguides are fabricated lithographically, and used the gas phase etching chemistry to narrow the ribbons down to $<$ 10 nm.[35] Wang *et al.* showed that two kinds of experimental techniques consisting of electron–beam sculpting and Joule heating were adopted and about 10-nm wide graphene nanoribbon waveguide was obtained.[36] The thinnest graphene nanoribbon structure obtained is about 1.6-nm wide with an estimated transport gap of about 400 meV.[36]

Inspired by this basic research, a dynamically tunable multiband PIT effect based on the graphene rectangle cavities coupled with a graphene nanoribbon waveguide is proposed by tuning the Fermi level of the graphene rectangle cavity. Two methods based on different physical mechanisms are used to realize a single-PIT effect; one is the bright and dark mode couplings through direct destructive interference, and the other is the cavity coupled with a graphene nanoribbon waveguide through indirect destructive interference. Moreover, dual- and triple-PIT effects are predicted in this ultra-compact structure, whereas the corresponding group indexes are controlled from 143.2 to 108.6 and 161.4 to 115.8. The problems on the PIT window with low transmission, single band, and untunability in plasmonic waveguide devices applied to integration can be worked out particularly well, thereby demonstrating a new door for the dynamic tuning of slow light and dynamically tunable multichannel light storage devices.

2. System model design and theoretical analysis

Figure 1 shows four types of models, which comprise remarkable graphene rectangle cavities and a graphene nanoribbon waveguide. The width of the graphene nanoribbon waveguide is only 10 nm in the PIT system because only the edge mode of the SPPs on the graphene nanoribbon is considered. In order to compensate for the difference between SPPs and vacuum wave vectors, the light source is coupled to the graphene nanoribbon waveguide through a grating or prism. In practical applications, a diffraction grating can be etched in the front of the waveguide to couple the light source into the graphene nanoribbon waveguide. In our paper, the edge modes are achieved by the transverse magnetic (TM) polarized SPPs modes placed in the x direction of the PIT system in Fig. 1. The incident light wave is restricted to travel forward in the waveguide when the incident light is injected and travels in the waveguide. SPPs are coupled into the graphene

rectangle cavity as the SPP wave passes through the cavity–waveguide coupling region due to the near-field coupling. The graphene nanoribbon waveguide and rectangle cavities are placed on a 200-nm thick sapphire substrate to avoid substrate loss in the mid-infrared band. Only propagation loss as low as 1.9 dB/cm at 5.18 μm are caused in silicon-on-sapphire (SOS) waveguide.[37] Al_2O_3 is selected as the substrate material mainly because of the low loss of SPPs that traveled on the sapphire in the THz band.[37] The refractive index of Al_2O_3 and Si are set as 1.59 and 3.95 used in the simulations, respectively. Here, the transmission spectrum of four types of models are simulated by using the finite-difference time domain (FDTD) method, and the calculated boundaries for structures are employed by the perfectly matched layer.

The length of the rectangle cavity is $w_a = w_b = w_c = w_d = 140$ nm, and the width of the rectangle cavity is $d_a = d_b = d_c = d_d = 20$ nm.[17] In addition, the coupling distance between the rectangle cavities and the graphene nanoribbon waveguide is $l_{a2} = 15$ nm, $l_{b1} = l_{b2} = 15$ nm, $l_{c1} = l_{c2} = l_{c3} = 15$ nm, $l_{d1} = l_{d3} = 15$ nm, and that between the bright and dark modes is $l_{a1} = l_{d2} = l_{d4} = 20$ nm.[17] The simulation results reveal that the Fermi level of the graphene nanoribbon waveguide is constantly maintained at 0.40 eV, and the Fermi level of the graphene rectangle cavity is tuned by changing the applied voltages.

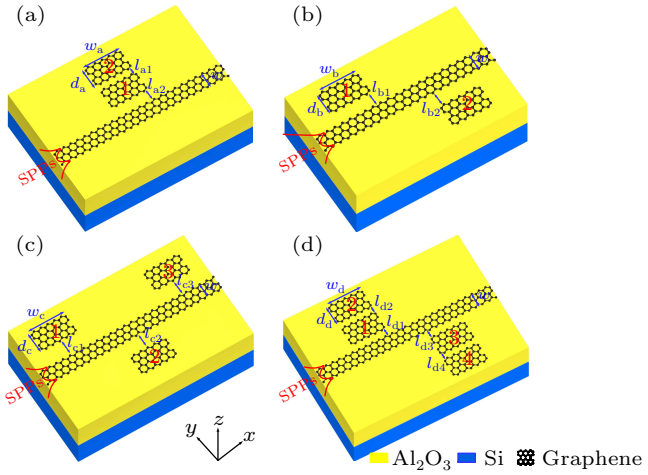


Fig. 1. The schematic diagram of the proposed two-cavity-coupled system [(a) and (b)], three-cavity-coupled system (c), and four-cavity-coupled system (d).

The conductivity of the single-layer graphene σ_g can be expressed by Kubo formula, which represents the sum of the interband and intraband contributions: $\sigma_g(\omega) = \sigma_{inter}(\omega) + \sigma_{intra}(\omega)$. The specific expression is as follows:[38]

$$\begin{aligned}\sigma_g(\omega) = & -\mathrm{i}\frac{e^2 k_B T}{\pi\hbar^2(\omega+\mathrm{i}\tau^{-1})} \\ & \times\left[\frac{E_F}{k_B T}+2\ln\left(\exp\left(-\frac{E_F}{k_B T}\right)+1\right)\right] \\ & -\mathrm{i}\frac{e^2}{4\pi\hbar^2}\times\ln\left[\frac{2|E_F|-\hbar(\omega+\mathrm{i}\tau^{-1})}{2|E_F|+\hbar(\omega+\mathrm{i}\tau^{-1})}\right], \end{aligned} \quad (1)$$

where i, T, k_B, e, τ, and $\hbar$ represent the imaginary unit, the temperature, the Boltzmann constant, the electron charge, the carrier relaxation time, and the Planck constant, respectively. ω is the angular frequency, E_F is the Fermi level of the graphene, and the main contributions of σ_g are from the intraband electron–photon scattering, whereas those of σ_g can be negligible from the direct transitions of the interband electron. Therefore, the conductivity σ_g of monolayer graphene can be obtained as a Drude-like expression after simplification[38,39]

$$\sigma_g = \frac{\mathrm{i}e^2 E_F}{\pi\hbar^2(\omega+\mathrm{i}\tau^{-1})}, \quad (2)$$

The carrier relaxation time $\tau = \mu_0 E_F/(ev_f^2)$, which is determined by the Fermi level of graphene E_F, the carrier mobility of graphene μ_0, and the Fermi velocity v_f ($\approx 10^6$ m/s). Here, it should be noticed that graphene is anisotropic and the out-of-plane permittivity is set as 2.5. In order to reduce the tremendous computation time in FDTD simulations, the mesh size inside the graphene layer is 0.2 nm, while non-uniform mesh size is employed to represent the other regions.

The propagation constant β of the monolayer graphene can be obtained using electromagnetic field boundary conditions and Maxwell equations to analyze the graphene properties effectively.[17]

$$\beta = k_0\sqrt{1-\left(\frac{2}{\eta_0\sigma_g}\right)^2}, \quad (3)$$

where k_0 and η_0 are the wavenumber and the impedance in the free space, respectively. Therefore, the effective refractive index is expressed by $n_{eff} = \beta/k_0$, and the intrinsic quality factor is $Q_{int} = \mathrm{Re}(n_{eff})/\mathrm{Im}(n_{eff})$.[36] Figure 2 shows the relationship of variation between the intrinsic quality factor and wavelength at various Fermi levels of the graphene. The intrinsic quality factor decreases with the respective increase in wavelength and the Fermi level of the graphene for the same wavelength, as shown in Fig. 2.

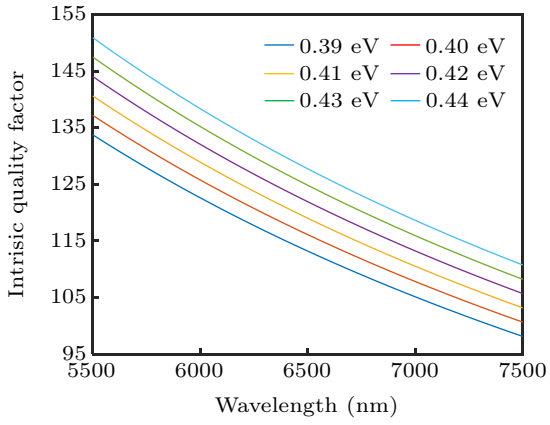


Fig. 2. Relationship between the intrinsic quality factor and the wavelength for various Fermi levels of the graphene $E_F = 0.39$, 0.40, 0.41, 0.42, 0.43, and 0.44 eV.

Graphene has an unparalleled advantage compared with noble metals due to its dynamic tunability. It is very easy to realize the Fermi level tuning via gate voltage, as described by the following formula:[38]

$$E_{\mathrm{F}} = \hbar v_{\mathrm{f}} \left(\frac{\pi \varepsilon_0 \varepsilon_{\mathrm{d}} V_{\mathrm{g}}}{d_{\mathrm{sub}} e} \right)^{1/2}, \tag{4}$$

where d_{sub} is the length between the graphene rectangle cavity and the substrate of Si, ε_0 is the vacuum permittivity, ε_{d} is the relative permittivity of dielectric silicon, and V_{g} is the applied bias voltage. This equation shows that the Fermi level of the monolayer graphene can be dynamically tuned by the bias voltage.

The Fermi level of the graphene rectangle cavity is tuned from 0.39 eV to 0.44 eV to obtain dynamically tunable and multiband PIT effect and multichannel slow light. The resonant wavelength of the graphene rectangle cavity can be expressed as follows:[17]

$$\lambda = 2\mathrm{Re}(n_{\mathrm{eff}})W/(m - \varphi/\pi), \tag{5}$$

where W is the coupling length between the graphene nanoribbon waveguide and the rectangle cavities, φ is the phase shift due to the reflection of the incident light in the cavity, and m is an integer.

3. Simulation results and discussion of single-PIT effect in bright and dark mode coupling systems

Figure 1(a) shows that the two-cavity-coupled system comprises rectangle cavity 1, rectangle cavity 2, and the graphene nanoribbon waveguide. The Fermi level of graphene rectangle cavities 1 and 2 is initially set as 0.40 eV and 0.42 eV, respectively. The bright mode can be directly activated by the SPPs wave, whereas the dark mode can be indirectly excited by the bright mode. In addition, the light can be coupled back to the bright mode, which results in the higher coupling strength between rectangle cavity 1 and graphene nanoribbon waveguide than that between cavity 2 and the waveguide. Therefore, cavities 1 and 2 behave as bright and dark modes, respectively.[40] Notably, the graphene-based nanoribbon waveguide, the graphene rectangle cavity 1, and the graphene rectangle cavity 2 can serve as the bare element $|1\rangle$, the dipole-allowed element $|2\rangle$, and the metastable element $|3\rangle$, respectively.[41] Two optical pathways, namely, $|1\rangle \rightarrow |2\rangle$ and $|1\rangle \rightarrow |2\rangle \rightarrow |3\rangle \rightarrow |2\rangle$, are observed in the proposed bright and dark mode coupling system. The bright cavity 1 and dark cavity 2 induce the transmission peaks because of the destructive interference with each other.

Figure 3 shows a schematic of the realizing principle according to the coupled mode theory (CMT) of the single-PIT effect in bright and dark mode coupling systems. The coupling mode equation is calculated, the single-PIT phenomena are analyzed, and the transmission and coupling loss of light wave are ignored. The dynamic equation of cavity mode amplitude a_i $(i = 1, 2)$ for the time-harmonic field $\mathrm{e}^{-\mathrm{j}\omega t}$ is as follows:[40]

$$\frac{\mathrm{d}a_1}{\mathrm{d}t} = (\mathrm{j}\omega_0 - \kappa_{\mathrm{int},1} - \kappa_{\mathrm{w}})\, a_1 + \sqrt{\kappa_{\mathrm{w}}} S^{(1)}_{+,\mathrm{in}} - \mathrm{j}\mu a_2, \tag{6}$$

$$\frac{\mathrm{d}a_2}{\mathrm{d}t} = (\mathrm{j}\omega_0 - \kappa_{\mathrm{int},2})\, a_2 - \mathrm{j}\mu a_1, \tag{7}$$

where $S^{(i)}_{\mathrm{p,in}}$ and $S^{(i)}_{\mathrm{p,out}}$ $(i = 1, 2)$ represent the transmitted waveguide mode amplitude of the input and output light waves, respectively, and the subscript $p = \pm$ represents propagation directions of the positive and negative the light waves. ω is the intrinsic resonant frequency of the bright and dark modes, $\kappa_{\mathrm{w},i} = 1/\tau_{\mathrm{w},i} = \omega_i/(2Q_{\mathrm{w},i})$ is the attenuation ratio on account of energy coupling to the graphene nanoribbon, $\kappa_{\mathrm{int},i} = 1/\tau_{\mathrm{int},i} = \omega_i/(2Q_{\mathrm{int},i})$ is the attenuation ratio on account of the intrinsic quality loss in the ith rectangle cavity, and $\mu = \omega_0/(2Q_{\mathrm{c}})$ is the coupling coefficient between the bright and dark mode. Q_{w}, $Q_{\mathrm{int},i}$, and Q_{c} are the waveguide coupling loss, the cavity quality factors related to the intrinsic loss, and the direct coupling between two rectangle cavities, respectively. FDTD simulation reveals the following: $Q_{\mathrm{int},1} = 113.2$, $Q_{\mathrm{int},2} = 122.5$, $Q_{\mathrm{t}} = 38.4$, $Q_{\mathrm{w}} = 58.17$, and $Q_{\mathrm{c}} = 16.7$.

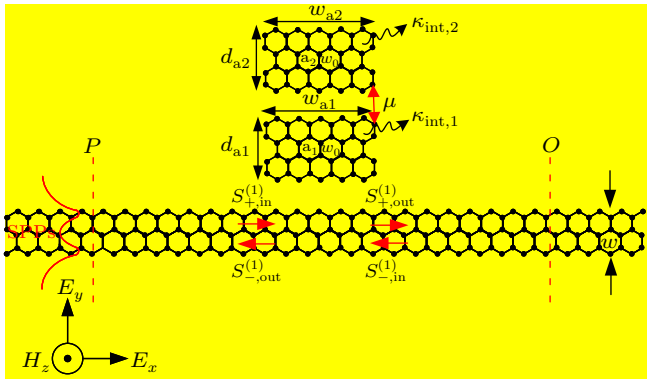


Fig. 3. The schematic diagram showing the realization of the principle of the single-PIT effect in bright and dark mode coupling systems.

The conservation of energy indicates that the output wave amplitude of each cavity can be expressed as follows:[41]

$$S^{(1)}_{+,\mathrm{out}} = S^{(1)}_{+,\mathrm{in}} - \sqrt{\kappa_{\mathrm{w}}} a_1, \tag{8}$$

$$S^{(1)}_{-,\mathrm{out}} = S^{(1)}_{-,\mathrm{in}} - \sqrt{\kappa_{\mathrm{w}}} a_1. \tag{9}$$

The output spectral transmission of the system for the coupling of bright and dark mode systems is as follows:[42]

$$T_1 = |t_{\mathrm{a}}|^2 = \left| \frac{S^{(1)}_{+,\mathrm{out}}}{S^{(1)}_{+,\mathrm{in}}} \right|^2$$

$$= \left| 1 - \frac{\kappa_{\mathrm{w}}}{\mathrm{j}(\omega - \omega_0) + \kappa_{\mathrm{int},1} + \kappa_{\mathrm{w}} + \frac{\mu^2}{\mathrm{j}(\omega-\omega_0)+\kappa_{\mathrm{int},2}}} \right|^2, \quad (10)$$

where t_{a} is the transmission coefficient of bright and dark mode coupling systems.

The transmission phase shift is $\theta(\omega) = \arg(t_{\mathrm{a}})$, and the group delay of this system is $\tau_{\mathrm{g}} = \partial\theta(\omega)/\partial\omega$. The slow light effect can be obtained by the group index n_{g}, which is derived by the following expression[22]

$$n_{\mathrm{g}} = \frac{c}{v_{\mathrm{g}}} = \frac{c}{l}\tau_{\mathrm{g}} = \frac{c}{l} \cdot \frac{\partial\theta(\omega)}{\partial\omega}, \quad (11)$$

where c, v_{g}, and l are the vacuum velocity of incident light, the group velocity, and the coupling length of monolayer graphene nanoribbon waveguide system, respectively.

The transmission spectra of the single-PIT effect under various graphene Fermi levels in bright and dark mode coupling systems are shown in Figs. 4(a1)–4(d1). The Fermi level of cavity 1 is constantly maintained as $E_{F1} = 0.40$ eV, while that of cavity 2 is set at different values $E_{F2} = 0.39$, 0.40, 0.41, and 0.42 eV. The transmission peak has an evident blue shift as the Fermi level of cavity 2 increases, and that of the PIT effect becomes slightly high, as shown in Figs. 4(a1)–4(d1). The data of the FDTD and CMT calculation are highly consistent. Consequently, the single-PIT effect can be dynamically tuned in this structure by tuning the Fermi level of cavity 2. Figures 4(a1) and 4(d1) show that the transmission peaks of the PIT effect are 58% and 66% when the Fermi level of cavity 2 is 0.39 eV and 0.42 eV, respectively. Therefore, the high transmittance of the single-PIT effect is maintained when the Fermi level of the graphene rectangle cavity is tuned from 0.39 eV to 0.42 eV. This finding indicates that the dynamically tunable single-PIT effect can be obtained by adjusting the Fermi level of the graphene rectangle cavity 2.

Figure 4(a2)–4(d2) show transmission phase shift responses and group index under various graphene Fermi levels (from 0.39 eV to 0.42 eV) in bright and dark mode coupling systems. Figures 4(a2)–4(d2) show that the phase shift is $2m\pi$ at the peak wavelength because the dispersions are strong in the transparent wavelength. The group index at the peak wavelength and the transmission peak wavelength of the PIT effect decrease with the increase of graphene Fermi level of cavity 2, as shown in Figs. 4(a2)–4(d2). Meanwhile, the intensity of the PIT transparent peak slightly decreases as the group index increases. This trend may be due to the additional time spent by the signal light in both rectangle cavities, thereby resulting in increased light power loss by scattering due to the resonance in the cavities. The group indexes of the peak wavelength are 74.9, 71.7, 69.6, and 66.1 with the graphene Fermi level of cavity 2 of 0.39, 0.40, 0.41, and 0.42 eV, respectively, as shown in the black dots of Figs. 4(a2)–4(d2).

Figure 5 shows that the magnetic field simulation of $|H_z|^2$ is depicted at the transmission peak wavelength to further understand the bright and dark mode coupling mechanism of this structure. This figure also reveals the magnetic field distribution at the peak wavelength of 6420 nm when the Fermi level of cavities 1 and 2 are set to 0.40 eV and 0.42 eV, respectively, and the corresponding transmission spectrum of the PIT effect is shown in Fig. 4(d1). The bright cavity is directly excited, whereas the dark cavity is activated by coupling with the bright one. Hence, only the dark cavity is efficiently activated, whereas the bright cavity is evidently suppressed at the transmission peak. Similar to the EIT effect in atom systems, canceling of the bright cavity is attributed to the destructive interference caused by two optical pathways from graphene nanoribbon waveguide to the graphene rectangle cavity.

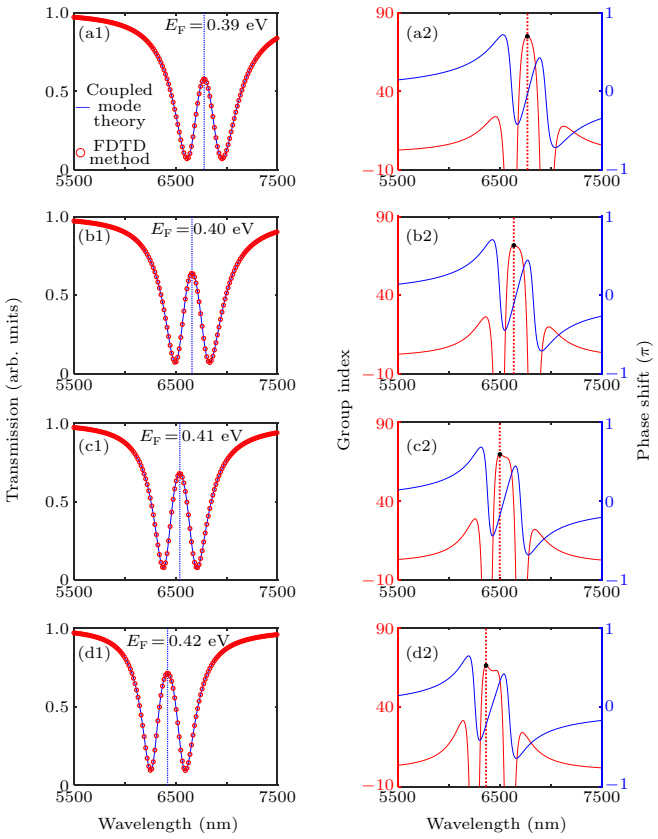


Fig. 4. Single-PIT effect simulation analysis of bright and dark mode coupling systems. (a1)–(d1) Transmission spectra of single-PIT effect. (a2)–(d2) Corresponding transmission phase shift responses and group index.

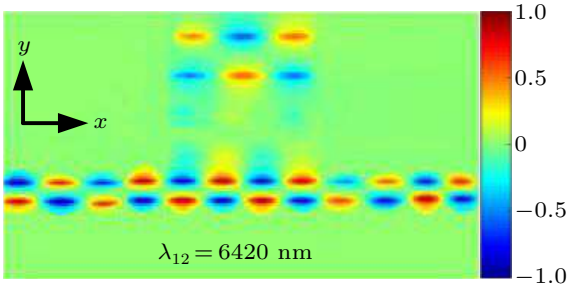


Fig. 5. $|H_z|^2$ magnetic field distributions of the single-PIT effect in bright and dark mode coupling systems at the transparent wavelength.

4. Simulation results and discussion of single-PIT effect in two cavities side-coupled with waveguide system

Figure 1(b) shows that the PIT system comprises rectangle cavities 1 and 2 side-coupled with a graphene nanoribbon waveguide. The Fermi levels of graphene rectangle cavities 1 and 2 are initially set to 0.40 eV and 0.44 eV, respectively. Figure 6 reveals the analysis of the dynamic transmission features for two cavities side-coupled with a graphene nanoribbon waveguide system using a temporal CMT. The normalized amplitude a_i for the time-harmonic field $e^{-j\omega t}$ of the ith cavity ($i = 1, 2$) for the time-harmonic field $e^{-j\omega t}$ is provided by the following expressions[16]

$$\frac{da_1}{dt} = (-j\omega_1 - \kappa_{int,1} - \kappa_{w,1})a_1 + \sqrt{\kappa_{w,1}}S^{(1)}_{+,in} + \sqrt{\kappa_{w,1}}S^{(1)}_{-,in}, \quad (12)$$

$$\frac{da_2}{dt} = (-j\omega_2 - \kappa_{int,2} - \kappa_{w,2})a_2 + \sqrt{\kappa_{w,2}}S^{(2)}_{+,in} + \sqrt{\kappa_{w,2}}S^{(2)}_{-,in}, \quad (13)$$

where ω_i ($i = 1, 2$) are the intrinsic resonant frequencies of the two cavities, $\kappa_{w,i}$ ($i = 1, 2$) is the attenuation ratio due to energy coupling into the plasmonic waveguide, and $\kappa_{int,i}$ ($i = 1, 2$) is the attenuation ratio of the i-th rectangle cavity; $Q_{w1} = 23.1$, $Q_{w2} = 22.5$, $Q_{int,1} = 127.7$, $Q_{int,2} = 132.2$, and $Q_t = 19.1$.

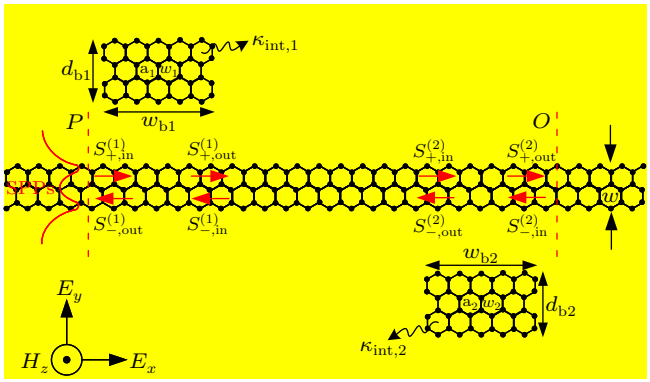


Fig. 6. Schematic diagram showing the realization of the principle of the single-PIT effect in two cavities side-coupled with a graphene nanoribbon waveguide.

The current study assumes the presence of only the light of the positive x direction ($S^{(2)}_{-,in} = 0$), and the transmission and reflection coefficients of a single cavity side-coupled with a graphene nanoribbon waveguide system are expressed as follows:

$$t_i(\omega) = \frac{j(\omega_i - \omega) + \kappa_{int,i}}{j(\omega_i - \omega) + \kappa_{int,i} + \kappa_{w,i}}, \quad (14)$$

$$r_i(\omega) = -\frac{\kappa_{w,i}}{j(\omega_i - \omega) + \kappa_{int,i} + \kappa_{w,i}}. \quad (15)$$

The output transmitted efficiency for the two graphene rectangle cavities side-coupled with a graphene nanoribbon waveguide system can be expressed as follows:[43]

$$T_2 = |t_b|^2 = \left|\frac{S^{(2)}_{+,out}}{S^{(1)}_{+,in}}\right|^2 = \left|\frac{t_1(\omega)t_2(\omega)}{1 - r_1(\omega)r_2(\omega)e^{j\phi}}\right|^2, \quad (16)$$

where t_b is the transmission coefficient of two graphene rectangle cavities side-coupled with a graphene nanoribbon waveguide system, and ϕ is the phase shift between two rectangle cavities.

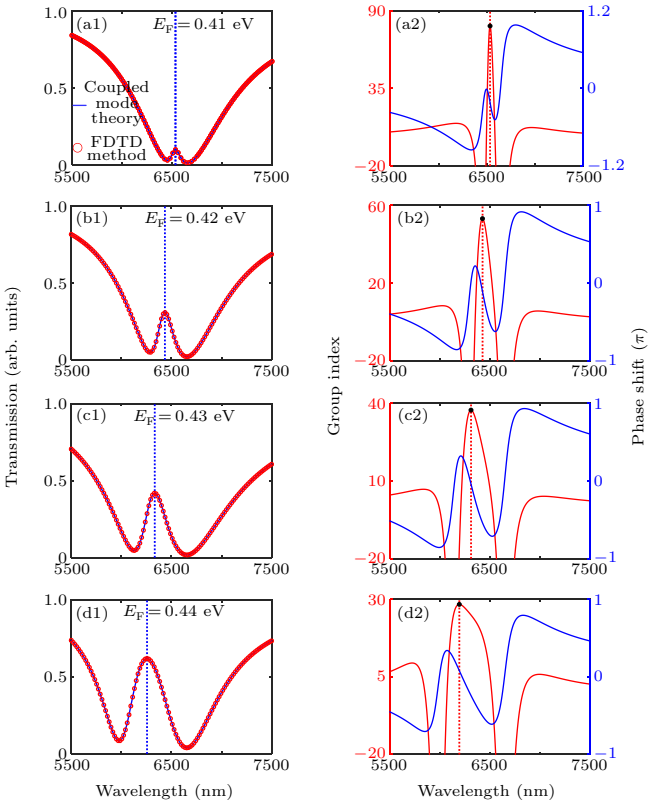


Fig. 7. Single-PIT effect simulation analysis of two cavities side-coupled with a graphene nanoribbon waveguide system. (a1)–(d1) Transmission spectrum of the single-PIT effect. (a2)–(d2) Corresponding transmission phase shift responses and group index.

Figure 7 shows the results of the transmission spectra, corresponding transmission phase shift responses, and group index under different graphene Fermi levels (from 0.41 eV to 0.44 eV). The resonant wavelength of rectangle cavity 2 is blueshifted as the graphene Fermi level of cavity 2 increases, and the wavelength detuning between the two cavities increases. The PIT peak wavelength blueshifts because of the reduction in effective refractive index. The transmission spectrum shows a PIT peak because of the strong coupling between two cavities and the phase shift value of $2m\pi$ (where m is an integer). Figures 7(a2)–7(d2) show that the transmission phase shift is 0 π at the peak wavelength due to the Fabry–Perot resonance. Figures 7(a1)–7(d1) reveal the gradual increase in transparent peak as the wavelength detuning increases, indicating an increase in coherent interference between the two rectangle cavities. Figure 7(a1) proves that the bandwidth is ultranarrow when the graphene Fermi level

of cavity 2 is 0.41 eV, and a low PIT peak is obtained. Figure 7(d1) shows that the bandwidth reaches a maximum when the graphene Fermi level of cavity 2 is increased to 0.44 eV, and the peak value of PIT reaches 62%. This result indicates that strong destructive interference is achieved between the two rectangle cavities.

The maximum delay of this PIT system is inversely proportional to the bandwidth of transmission because of the principle of the delay bandwidth product, resulting in a tradeoff between the group index and wavelength detuning. Thus, the group index decreases as the wavelength detuning increases at the peak wavelength, as indicated in Figs. 7(a2)–7(d2). Meanwhile, the intensity of the PIT transparent peak decreases as the group index increases. This phenomenon is due to the additional time spent by the signal light in both rectangle cavities, resulting in increased light power loss by resonance in the cavities. The group indexes of the peak wavelength are 79.2, 53.2, 37.4, and 28.3 with the graphene Fermi levels of cavity 2 of 0.41, 0.42, 0.43, and 0.44 eV, respectively, as shown in the black dots of Figs. 7(a2)–7(d2).

Figures 8(a)–8(c) show that the magnetic field simulation of $|H_z|^2$ is depicted at the transmission peak and the two dip wavelengths to further understand the coupling mechanism of this structure. Figure 8(a) demonstrates the magnetic field distribution at the resonance wavelength of cavity 1 at 6650 nm when the Fermi levels of cavities 1 and 2 are set to 0.40 eV and 0.44 eV, respectively. Figure 8(b) shows the magnetic field distribution at the peak wavelength of the PIT effect at 6256 nm, and the corresponding transmission spectrum of the PIT effect is presented in Fig. 7(d1). Figure 8(c) shows the magnetic field distribution at the resonant wavelength of cavity 2 at 5983 nm. The results show that Fabry–Perot resonance exists between the two rectangle cavities.

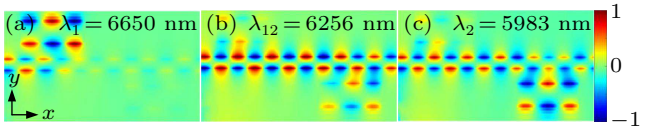


Fig. 8. $|H_z|^2$ magnetic field distributions of the single-PIT effect in two cavities side-coupled with a graphene nanoribbon waveguide system at the resonance wavelength.

Table 1 shows the maximum transmission and group index of the single-PIT system under different Fermi levels of graphene rectangle cavities at the peak wavelength of PIT. The maximum transmission of the single-PIT effect of bright and dark mode coupling systems is tuned from 58% to 71% due to the changing Fermi level of the graphene rectangle cavity 2 from 0.39 eV to 0.42 eV, and the group index is controlled between 74.9 and 66.1. This condition indicates that a fine-tuning method of the group index can be obtained in this PIT system. Alternatively, the maximum transmission of the single-PIT effect of two cavities side-coupled with a graphene nanoribbon waveguide system is tuned from 10% to 62% due to the changing Fermi level of the graphene rectangle cavity 2 from 0.41 eV to 0.44 eV, and the group index is controlled between 79.2 and 28.3. This condition indicates that the group index is tuned in a large tuning range by dynamically tuning the Fermi level of the graphene rectangle cavity. These results can be effectively applied to dynamically tunable light storage and slow light devices.

Table 1. Maximum transmission and group index of the single-PIT system under different Fermi levels of graphene rectangle cavities at the peak wavelength of PIT.

System model	Fermi levels of graphene rectangle cavities (eV)	Maximum transmission of PIT peak (%)	Maximum group index of PIT system
Single-PIT effect of bright and dark mode coupling system	$E_{F1} = 0.40$, $E_{F2} = 0.39$	58	74.9
	$E_{F1} = 0.40$, $E_{F2} = 0.40$	64	71.7
	$E_{F1} = 0.40$, $E_{F2} = 0.41$	67	69.6
	$E_{F1} = 0.40$, $E_{F2} = 0.42$	71	66.1
Single-PIT effect of two cavities side-coupled with a waveguide system	$E_{F1} = 0.40$, $E_{F2} = 0.41$	10	79.2
	$E_{F1} = 0.40$, $E_{F2} = 0.42$	31	53.2
	$E_{F1} = 0.40$, $E_{F2} = 0.43$	41	37.4
	$E_{F1} = 0.40$, $E_{F2} = 0.44$	62	28.3

5. Simulation results and discussion of dual-PIT effect in triple cavities side-coupled with a graphene nanoribbon waveguide system

Figure 1(c) shows that the dual PIT system comprises rectangle cavity 1, cavity 2, cavity 3, and a graphene nanoribbon waveguide. The graphene rectangle cavity 1, cavity 2, and cavity 3 have an initial Fermi level of 0.42, 0.43, and 0.44 eV, respectively. Figure 9 shows that the dynamic transmission features for triple graphene rectangle cavities side-coupled with a graphene nanoribbon waveguide system are analyzed by a temporal CMT. The normalized amplitude a_i for the time-harmonic field $e^{-j\omega t}$ of the i-th cavity ($i = 1, 2, 3$) are analyzed by the following

$$\frac{da_1}{dt} = (j\omega_1 - \kappa_{int,1} - \kappa_{w,1})\, a_1 + \sqrt{\kappa_{w,1}} S^{(1)}_{+,in} + \sqrt{\kappa_{w,1}} S^{(1)}_{-,in}, \quad (17)$$

$$\frac{\mathrm{d}a_2}{\mathrm{d}t} = (\mathrm{j}\omega_2 - \kappa_{\mathrm{int},2} - \kappa_{\mathrm{w},2})a_2 + \sqrt{\kappa_{\mathrm{w},2}}S^{(2)}_{+,\mathrm{in}} + \sqrt{\kappa_{\mathrm{w},2}}S^{(2)}_{-,\mathrm{in}}, \tag{18}$$

$$\frac{\mathrm{d}a_3}{\mathrm{d}t} = (\mathrm{j}\omega_3 - \kappa_{\mathrm{int},3} - \kappa_{\mathrm{w},3})a_3 + \sqrt{\kappa_{\mathrm{w},3}}S^{(3)}_{+,\mathrm{in}} + \sqrt{\kappa_{\mathrm{w},3}}S^{(3)}_{-,\mathrm{in}}, \tag{19}$$

where ω_i ($i = 1, 2, 3$) represents the intrinsic resonant frequencies of the three cavities, $\kappa_{\mathrm{int},i}$ ($i = 1, 2, 3$) is the attenuation ratio of the i-th rectangle cavity, and $\kappa_{\mathrm{w},i}$ ($i = 1, 2, 3$) is the attenuation ratio due to energy coupling into the graphene nanoribbon waveguide.

The conservation of energy indicates that the output wave amplitude of each rectangle cavity can be analyzed ($i = 1, 2$), as follows:

$$S^{(i)}_{+,\mathrm{out}} = S^{(i+1)}_{+,\mathrm{in}}\mathrm{e}^{\mathrm{j}\phi_i/2}, \tag{20}$$

$$S^{(i+1)}_{-,\mathrm{out}} = S^{(i)}_{-,\mathrm{in}}\mathrm{e}^{\mathrm{j}\phi_i/2}, \tag{21}$$

where ϕ_1 is the transmission phase shift between cavities 1 and 2, and ϕ_2 is the transmission phase shift between cavities 2 and 3 ($\phi_1 = \phi_2 = \phi$).

The output transmitted efficiency for triple graphene rectangle cavities side-coupled with a graphene nanoribbon waveguide system can be analyzed as follows:

$$T_3 = |t_{\mathrm{c}}|^2 = \left|\frac{S^{(3)}_{+,\mathrm{out}}}{S^{(1)}_{+,\mathrm{in}}}\right|^2 = \left|\frac{\alpha_1\alpha_2\alpha_3}{(\alpha_1+\kappa_{\mathrm{w},1})(\alpha_3+\kappa_{\mathrm{w},3})\alpha_2\mathrm{e}^{\mathrm{j}\phi} - \kappa_{\mathrm{w},1}\kappa_{\mathrm{w},3}\alpha_2\mathrm{e}^{-\mathrm{j}\phi} + (\alpha_1+\kappa_{\mathrm{w},1})(\kappa_{\mathrm{w},2}\alpha_3\mathrm{e}^{\mathrm{j}\phi} + \kappa_{\mathrm{w},1}\kappa_{\mathrm{w},3}\mathrm{e}^{\mathrm{j}\phi} - 1) - \kappa_{\mathrm{w},1}\kappa_{\mathrm{w},2}\alpha_3 + \kappa_{\mathrm{w},1}\kappa_{\mathrm{w},2}\kappa_{\mathrm{w},3}(\mathrm{e}^{-\mathrm{j}\phi} - 1)}\right|^2, \tag{22}$$

where $\alpha_1 = \mathrm{j}(\omega - \omega_1) + \kappa_{\mathrm{int},1}$, $\alpha_2 = \mathrm{j}(\omega - \omega_2) + \kappa_{\mathrm{int},2}$, $\alpha_3 = \mathrm{j}(\omega - \omega_3) + \kappa_{\mathrm{int},3}$; t_{c} is the transmission coefficient of triple graphene rectangle cavities side-coupled with a graphene nanoribbon waveguide system.

FDTD simulations revealed that the corresponding resonant wavelengths of rectangle cavities 1, 2, and 3 are [6815, 6625, and 6435 nm], [6650, 6460, and 6270 nm], [6483, 6293, and 6103 nm], and [6324, 6134, and 5944 nm] when Fermi levels of graphene rectangle cavities 1, 2, and 3 are [0.39, 0.40, and 0.41 eV], [0.40, 0.41, and 0.42 eV], [0.41, 0.42, and 0.43 eV], and [0.42, 0.43, and 0.44 eV]. The corresponding intrinsic quality factors are presented in Fig. 2. The total quality factors are caused by the following two PIT transparent peaks. The total quality factor Q_{t} of the graphene rectangle cavity can be calculated from $Q_{\mathrm{t}} = \lambda_0/\Delta\lambda$, where λ_0 and $\Delta\lambda$ are the peak wavelength and full width at half maximum of the reflection spectrum, respectively. Therefore, the corresponding coupling quality factors of rectangle cavities 1, 2, and 3 can be obtained in accordance with $Q_{\mathrm{w}} = Q_{\mathrm{int}}Q_{\mathrm{t}}/(Q_{\mathrm{int}} - Q_{\mathrm{t}})$, as shown in Table 2.

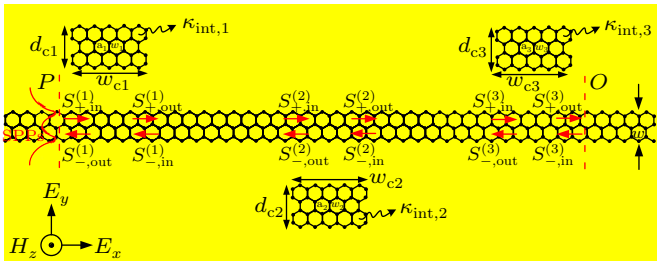


Fig. 9. Schematic diagram showing the realization of the principle of the dual-PIT effect in triple cavities side-coupled with a waveguide system.

Table 2. Q_{int}, Q_{t}, and Q_{w} under different Fermi levels of graphene rectangle cavities in triple cavities side-coupled with a graphene nanoribbon waveguide system.

Fermi levels of graphene rectangle cavities (eV)	The corresponding intrinsic quality factors	The total quality factors	The corresponding coupling quality factors
$E_{\mathrm{F1}} = 0.39$, $E_{\mathrm{F2}} = 0.40$, $E_{\mathrm{F3}} = 0.41$	$Q_{\mathrm{int},1} = 108.2$, $Q_{\mathrm{int},2} = 113.5$, $Q_{\mathrm{int},3} = 120.1$	$Q_{\mathrm{t},1} = 90.2, 88.5$	$Q_{\mathrm{w},1} = 540.1$, $Q_{\mathrm{w},2} = 432.2$, $Q_{\mathrm{w},3} = 329.2$
$E_{\mathrm{F1}} = 0.40$, $E_{\mathrm{F2}} = 0.41$, $E_{\mathrm{F3}} = 0.42$	$Q_{\mathrm{int},1} = 113.4$, $Q_{\mathrm{int},2} = 120.1$, $Q_{\mathrm{int},3} = 126.5$	$Q_{\mathrm{t},2} = 80.4, 77.6$	$Q_{\mathrm{w},1} = 272.8$, $Q_{\mathrm{w},2} = 223.1$, $Q_{\mathrm{w},3} = 197.1$
$E_{\mathrm{F1}} = 0.41$, $E_{\mathrm{F2}} = 0.42$, $E_{\mathrm{F3}} = 0.43$	$Q_{\mathrm{int},1} = 120.1$, $Q_{\mathrm{int},2} = 126.1$, $Q_{\mathrm{int},3} = 132.9$	$Q_{\mathrm{t},3} = 72.7, 70.3$	$Q_{\mathrm{w},1} = 184.2$, $Q_{\mathrm{w},2} = 159.8$, $Q_{\mathrm{w},3} = 149.5$
$E_{\mathrm{F1}} = 0.42$, $E_{\mathrm{F2}} = 0.43$, $E_{\mathrm{F3}} = 0.44$	$Q_{\mathrm{int},1} = 125.2$, $Q_{\mathrm{int},2} = 132.3$, $Q_{\mathrm{int},3} = 139.7$	$Q_{\mathrm{t},4} = 65.6, 63.4$	$Q_{\mathrm{w},1} = 137.2$, $Q_{\mathrm{w},2} = 130.3$, $Q_{\mathrm{w},3} = 116.3$

Figure 10(d1) shows that A, B, and C are the corresponding transmission dips when the Fermi levels of rectangle cavities 1, 2, and 3 are 0.42, 0.43, and 0.44 eV, respectively. Peak I is the PIT transparent peak, which is caused by the light resonance in cavities 2 and 3. The amplitude of the input wave in cavity 1 is equal to that in cavity 2 because the light is not coupled into cavity 1. Therefore, $S^{(1)}_{+,\mathrm{in}} = S^{(2)}_{+,\mathrm{in}}$, and $T_3' = |S^{(3)}_{+,\mathrm{out}}/S^{(2)}_{+,\mathrm{in}}|^2$. Similarly, peak II, which is caused by the resonance of the light in cavities 1 and 2, is the PIT transparent peak. The amplitude of the output wave in cavity 2 is equal to

that in cavity 3 because the light is not coupled into cavity 3. Herein, $S^{(2)}_{+,\mathrm{out}} = S^{(3)}_{+,\mathrm{out}}$, and $T_3'' = |S^{(2)}_{+,\mathrm{out}}/S^{(1)}_{+,\mathrm{in}}|^2$.

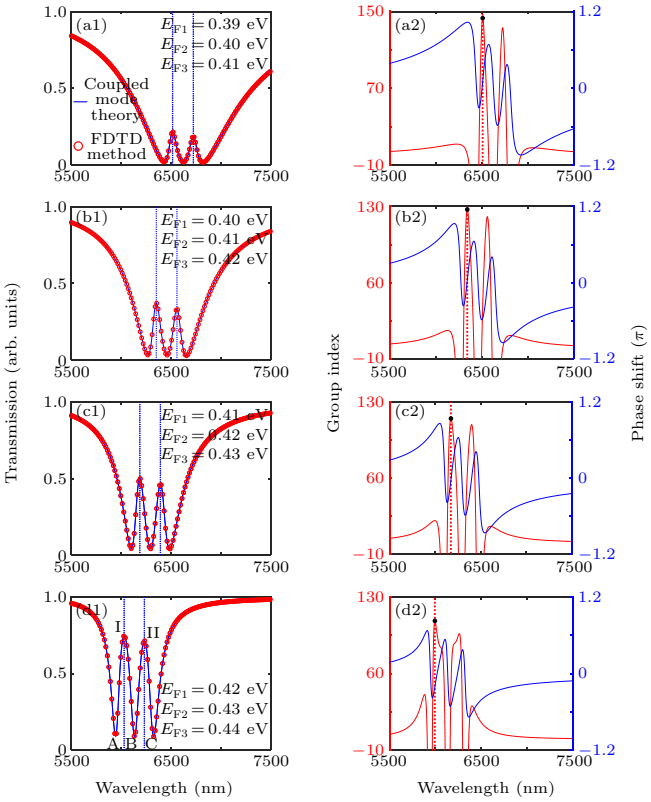


Fig. 10. Dual-PIT effect simulation analysis of triple cavities side-coupled with a graphene nanoribbon waveguide system. (a1)–(d1) Transmission spectra of the dual-PIT effect. (a2)–(d2) Corresponding transmission phase shift responses and group indexes.

Figures 10(a1)–10(d1) show the normalized transmission intensity spectra of the dual-PIT effect under various Fermi levels of graphene rectangle cavities. The resonant wavelengths of cavities 1, 2, and 3 show a blue shift, and the two PIT transmission peaks increase with the Fermi levels of graphene rectangle cavities, as shown in Figs. 10(a1)–10(d1). The transmission peaks I and II of the dual-PIT effect are the minimum values of only 21% and 18%, respectively, when the Fermi levels of graphene rectangle cavities 1, 2, and 3 are 0.39, 0.40, and 0.41 eV, respectively, as shown in Fig. 10(a1). However, the values of the transmission peaks I and II can reach 74% and 71%, respectively, when the Fermi levels of graphene rectangle cavities 1, 2, and 3 are 0.42, 0.43, and 0.44 eV, respectively, as shown in Fig. 10(d1). These results indicate that the dual-PIT effect can be effectively tuned by adjusting the Fermi level of the graphene rectangle cavity.

Figures 10(a2)–10(d2) show the transmission spectrum phase shifts and group indexes of dual-PIT effect with the change in the Fermi level of graphene rectangle cavity. The results reveal the aggressive phase changes of the dual-PIT windows. The strong destructive interference near the peak of the transparency in the monolayer graphene-PIT structure results in a drastic dispersion. Hence, this phenomenon can induce a phase mutation, and the round-trip phase difference between the two cavities in the PIT system is an integer multiple of 2π. The transmission phase shifts of the dual-PIT effect caused by the light resonance in cavities 1 and 2 as well as cavities 2 and 3 are 0π. The dispersions are normal in the three cavity systems. Then, the phase dispersion results in a change in the group index. The group index of the dual-PIT system increases with the decrease in the Fermi level of the graphene rectangle cavity, and the two transmission peaks decrease, as shown in Figs. 10(a2)–10(d2). This trend is due to the additional time spent by the signal light in resonance between cavities 1 and 2 as well as that between cavities 2 and 3, resulting in increased optical power loss among the three rectangle cavities. Therefore, the output light intensity of the dual-PIT system decreases with the graphene Fermi level. Moreover, a large group index is always maintained at the peak wavelength of the dual-PIT system. The corresponding maximum group indexes are 143.2, 127.3, 116.2, and 108.6, as shown in the black dots of Figs. 10(a2)–10(d2). These results can be applied to dynamically tunable two-channel optical filters, optical modulators,[44] and slow light devices because of high transmission and ultranarrow bandwidth.[12]

The field distributions of $|H_z|^2$ at the two peak wavelengths are depicted by simulation at the transmission peak wavelengths, as shown in Figs. 11(a) and 11(b) to further understand the dual-PIT effect mechanism of this structure. Herein, the Fermi levels of rectangle cavities 1, 2, and 3 are 0.42, 0.43, and 0.44 eV, respectively. Figure 11(a) shows the magnetic field distribution at the peak wavelength of $\lambda_{12} = 6232$ nm when the light is resonated between cavities 1 and 2. Moreover, figure 11(b) shows the magnetic field distribution at the peak wavelength of $\lambda_{23} = 6029$ nm when the light is resonated between cavities 2 and 3. The corresponding transmission spectrum of the dual-PIT effect is shown in Fig. 10(d1). The results indicate that the three rectangle cavities act as three resonators, and the Fabry–Perot resonance is realized between cavities 1 and 2 or cavities 2 and 3. Therefore, the formation mechanism of the dual PIT effect is the same as that of the single PIT effect, which is caused by resonance between two rectangle cavities.

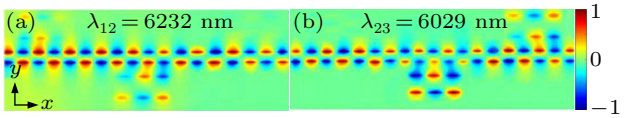


Fig. 11. $|H_z|^2$ magnetic field distributions of the dual-PIT effect in triple cavities side-coupled with a graphene nanoribbon waveguide system at the peak wavelength.

6. Simulation results and discussion of triple-PIT system

Figure 1(d) shows that the triple PIT system comprises rectangle cavities 1, 2, 3, 4, and the graphene nanoribbon waveguide. The triple-PIT effect is also obtained by the combination of a bright and dark mode coupling and the cavities

side-coupled with a graphene nanoribbon waveguide mechanism. The Fermi levels of graphene rectangle cavities 1, 2, 3, and 4 are initially set to 0.40, 0.42, 0.42, and 0.44 eV, respectively. The dynamic transmission characteristics for the triple-PIT system in Figure 12 are analyzed by a temporal CMT. The normalized amplitude a_i for the time-harmonic field $e^{-j\omega t}$ of the i-th cavity ($i = 1, 2, 3, 4$) are given by the following equations

$$\frac{da_1}{dt} = (j\omega_{01} - \kappa_{int,1} - \kappa_{w,1})a_1 + \sqrt{\kappa_{w,1}}S^{(1)}_{+,in} + \sqrt{\kappa_{w,1}}S^{(1)}_{-,in} - j\mu_{12}a_2, \quad (23)$$

$$\frac{da_2}{dt} = (j\omega_{01} - \kappa_{int,2})a_2 - j\mu_{12}a_1, \quad (24)$$

$$\frac{da_3}{dt} = (j\omega_{02} - \kappa_{int,3} - \kappa_{w,3})a_3 + \sqrt{\kappa_{w,3}}S^{(2)}_{+,in} + \sqrt{\kappa_{w,3}}S^{(2)}_{-,in} - j\mu_{34}a_4, \quad (25)$$

$$\frac{da_4}{dt} = (j\omega_{02} - \kappa_{int,4})a_4 - j\mu_{34}a_3, \quad (26)$$

where ω_{01} is the intrinsic resonant frequency of cavities 1 and 2, and ω_{02} is the intrinsic resonant frequency of cavities 3 and 4. $\kappa_{w,i}$ ($i = 1, 3$) is the attenuation ratio due to energy coupling into the graphene nanoribbon waveguide, and $\kappa_{int,i}$ ($i = 1, 2, 3, 4$) is the attenuation ratio of the i-th rectangle cavity. $\mu_{12} = \omega_{01}/(2Q_{c,1})$ and $\mu_{34} = \omega_{02}/(2Q_{c,2})$ are the coupling coefficients between cavities 1 and 2 and between cavities 3 and 4, respectively. $Q_{w,i}$ ($i = 1, 3$), $Q_{int,i}$ ($i = 1, 2, 3, 4$), and $Q_{c,i}$ ($i = 1, 2$) are the waveguide coupling loss, cavity quality factors due to the intrinsic loss, and direct coupling between bright and dark modes, respectively.

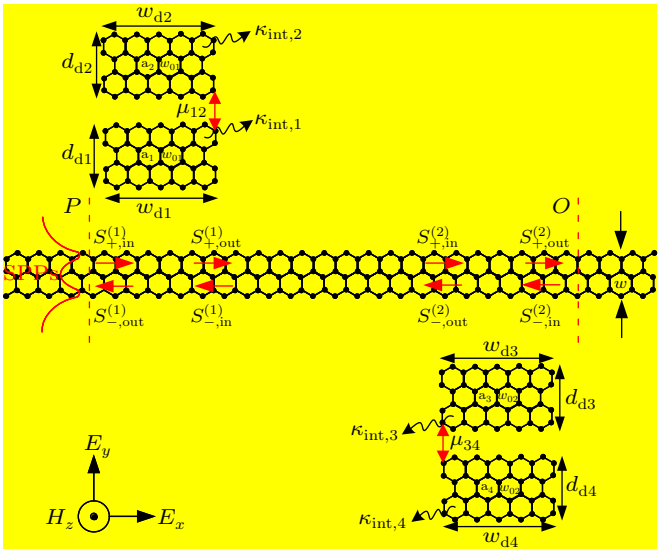


Fig. 12. Schematic diagram of the realizing principle of the triple-PIT system.

The energy conservation of the output wave amplitude in each cavity indicates that the output spectral transmittance of the system for the triple-PIT system is as follows:

$$T_4 = |t_d|^2 = \left|\frac{S^{(2)}_{+,out}}{S^{(1)}_{+,in}}\right|^2 = \left|\frac{(\beta_3 + (\mu^2_{34}/\beta_4))(\beta_1 + (\mu^2_{12}/\beta_2))}{(\beta_1 + \kappa_{w,1} + (\mu^2_{12}/\beta_2))(\beta_3 + \kappa_{w,3} + (\mu^2_{34}/\beta_4))e^{j\phi} - \kappa_{w,1}\kappa_{w,3}e^{-j\phi}}\right|^2, \quad (27)$$

where $\beta_1 = j(\omega - \omega_{01}) + \kappa_{int,1}$, $\beta_2 = j(\omega - \omega_{01}) + \kappa_{int,2}$, $\beta_3 = j(\omega - \omega_{02}) + \kappa_{int,3}$, $\beta_4 = j(\omega - \omega_{02}) + \kappa_{int,4}$, and t_d are the transmission coefficients of the triple-PIT system.

The total quality factors are caused by the triple-PIT transparent peaks. The corresponding intrinsic quality factors, total quality factors, and the coupling quality factors of rectangle cavities 1 and 3 are shown in Table 3. Herein, $Q_{c,1} = 42.13$, 41.85, 41.27, 40.93, and $Q_{c,2} = 41.43$, 41.12, 40.87, 40.46.

Table 3. Q_{int}, Q_t, and Q_w under different Fermi levels of graphene rectangle cavities triple-PIT system.

Fermi levels of graphene rectangle cavities (eV)	The corresponding intrinsic quality factors	The total quality factors	The corresponding coupling quality factors
$E_{F1} = 0.40$, $E_{F2} = 0.39$, $E_{F3} = 0.42$, $E_{F4} = 0.41$	$Q_{int,1} = 119.5$, $Q_{int,2} = 116.2$, $Q_{int,3} = 117.1$, $Q_{int,4} = 113.3$	$Q_{t,1} = 44.36$, $Q_{t,3} = 47.88$	$Q_{w,1} = 71.02$, $Q_{w,3} = 81.00$
$E_{F1} = 0.40$, $E_{F2} = 0.40$, $E_{F3} = 0.42$, $E_{F4} = 0.42$	$Q_{int,1} = 123.1$, $Q_{int,2} = 122.5$, $Q_{int,3} = 119.2$, $Q_{int,4} = 119.6$	$Q_{t,1} = 43.21$, $Q_{t,3} = 47.04$	$Q_{w,1} = 66.57$, $Q_{w,3} = 77.71$
$E_{F1} = 0.40$, $E_{F2} = 0.41$, $E_{F3} = 0.42$, $E_{F4} = 0.43$	$Q_{int,1} = 124.3$, $Q_{int,2} = 131.2$, $Q_{int,3} = 121.7$, $Q_{int,4} = 125.6$	$Q_{t,1} = 42.37$, $Q_{t,3} = 46.19$	$Q_{w,1} = 64.28$, $Q_{w,3} = 74.44$
$E_{F1} = 0.40$, $E_{F2} = 0.42$, $E_{F3} = 0.42$, $E_{F4} = 0.44$	$Q_{int,1} = 127.8$, $Q_{int,2} = 136.1$, $Q_{int,3} = 124.2$, $Q_{int,4} = 133.5$	$Q_{t,1} = 41.50$, $Q_{t,3} = 45.32$	$Q_{w,1} = 61.46$, $Q_{w,3} = 71.36$

Figure 13(d1) shows that peak I is the PIT transparent peak obtained by the bright and dark mode coupling mechanism attributed to the light resonance in cavities 1 and 2. The amplitude of the output wave in cavities 1 and 2 is equal to that in cavities 3 and 4 because the light is not coupled into cavities 3 and 4. Hence, $S^{(1)}_{+,out} = S^{(2)}_{+,out}$, and $T'_4 = |S^{(1)}_{+,out}/S^{(1)}_{+,in}|^2$. In-

stead, peak II is the PIT transparent peak based on the cavities side-coupled with a graphene nanoribbon waveguide mechanism attributed to the light resonance in cavities 1 and 3. Consequently, $T_4'' = |S^{(2)}_{+,\text{out}}/S^{(1)}_{+,\text{in}}|^2$. Similar to peak I, peak III is the PIT transparent peak based on the mechanism of the bright and dark mode coupling caused by the light resonance in cavities 3 and 4. The amplitude of the input wave in cavities 1 and 2 is equal to that in cavities 3 and 4 because the light is not coupled into cavities 1 and 2. Therefore, $S^{(1)}_{+,\text{in}} = S^{(2)}_{+,\text{in}}$, and $T_4''' = |S^{(2)}_{+,\text{out}}/S^{(2)}_{+,\text{in}}|^2$.

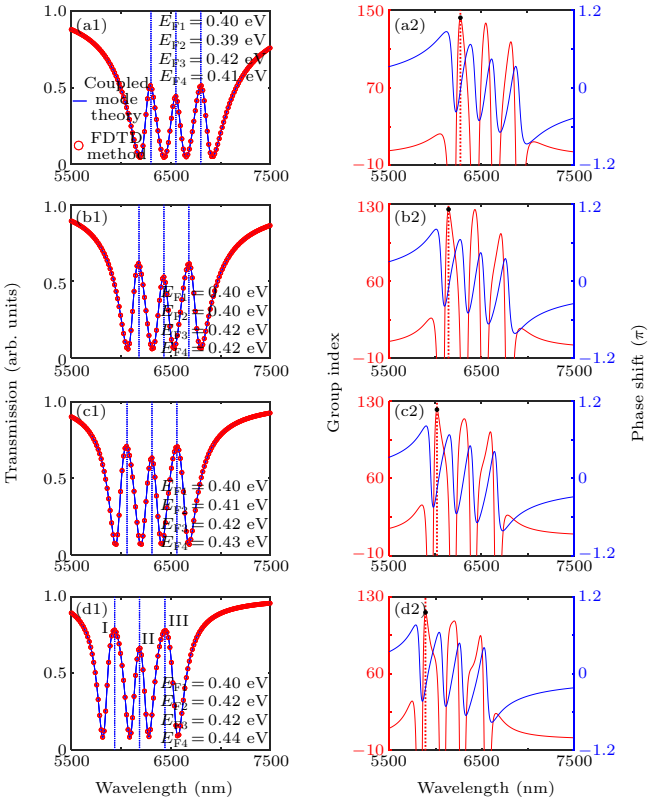


Fig. 13. Triple-PIT effect simulation analysis. (a1)–(d1) Transmission spectra of the triple-PIT effect. (a2)–(d2) Corresponding phase-shift responses and group indexes.

Figures 13(a1)–13(d1) show the normalized transmission intensity spectra of triple-PIT effect under various Fermi levels of graphene rectangle cavities. The peak wavelengths show a blue shift, and the triple-PIT transmission peaks increase with the Fermi levels of graphene rectangle cavities, as shown in Figs. 13(a1)–13(d1). Figure 13(a1) shows that the transmission peaks I, II, and III of the triple-PIT effect are the minimum values of 51%, 44%, and 51%, respectively, when the Fermi levels of graphene rectangle cavities 1, 2, 3, and 4 are 0.40, 0.39, 0.42, and 0.41 eV, respectively Meanwhile, the values of the transmission peaks I, II, and III can reach 74%, 65%, and 73%, respectively. These results are attributed to the strengthened coupling strength, which is affected by the resonance between the bright and dark modes and the resonance between rectangle cavities and a graphene nanoribbon waveguide when the Fermi levels of graphene rectangle cavities 1, 2, 3, and 4 are 0.40, 0.42, 0.42, and 0.44 eV, respectively, as shown in Fig. 13(d1). Therefore, the triple-PIT effect can be effectively tuned by adjusting the Fermi level of the graphene rectangle cavity.

Figures 13(a2)–13(d2) show the transmission spectrum phase shifts and group indexes of triple-PIT effect with the change in the Fermi level of graphene rectangle cavity. The group index sharply drops due to the sudden change in the phase shift at the transmission dip. A 2π phase shift exists at the peak wavelength, and the highest group index reaches 161.4. Hence, a large group index is obtained near the transmission dip due to the strong dispersion. The corresponding frequency light signal remains longer than other frequencies when it travels in this structure. This feature enables the device to be used in optical storage applications. If the Fermi level of the dark mode of cavities 2 and 4 is tuned to differ from the bright mode of cavities 1 and 3 by varying applied voltage attached to graphene, then the group index increases, and the corresponding maximum group indexes are 161.4, 144.8, 131.4, and 115.8, as shown in the black dots of Figs. 13(a2)–13(d2). Thus, the triple-PIT phenomenon can be effectively modulated to seek the desired slow light effect. These results can be applied to dynamically tunable three-channel optical filters,[6] optical modulators,[44] sensors,[45] switching,[46,47] and slow light devices[11] with high transmission, ultranarrow bandwidth, and good slow light effect.

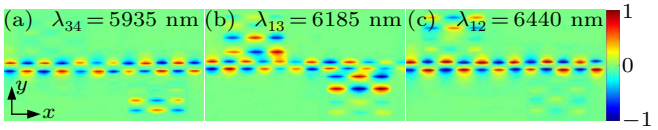


Fig. 14. $|H_z|^2$ magnetic field distributions of the triple-PIT effect at the peak wavelength.

Figures 14(a)–14(c) show the field distributions of $|H_z|^2$ at the three peak wavelengths represented by I, II, and III by using the FDTD method in Fig. 13(d1) to further understand the triple-PIT effect mechanism of this structure. The field distributions of $|H_z|^2$ shown in Figs. 14(a) and 14(c) demonstrate that the strongly destructive interference between the bright and dark cavities produced the transmission peaks I and III, thereby enabling the propagation of the SPP wave through the structure without limitation. Notably, the dark cavity is activated strongly, and the magnetic field of the bright cavity is activated weakly at 5935 nm and 6440 nm. Therefore, the drastic excitation of the dark cavity can destructively restrain the oscillation of the bright cavity. Moreover, the occurrence of the transmission peak II at 6185 nm is very different from that of peaks I and III because all bright cavities are activated simultaneously, as shown in Fig. 14(b). Meanwhile, the bright-dark mode and waveguide couplings between the cavities below and above the graphene nanoribbon waveguide affect the transmission spectrum simultaneously. The formation

of transmission peak II is due to the destructive interference between the magnetic fields of cavities below and above the graphene nanoribbon waveguide.

Table 4 shows the maximum transmission and group index of the dual and triple-PIT systems under different Fermi levels of graphene rectangle cavities and pump light intensity at the peak wavelength of PIT. The transmission peak of the dual-PIT effect is tuned from 21% to 74% and the group index of the dual PIT system is controlled between 143.2 and 108.6 when the Fermi levels of graphene rectangle cavities 1, 2, and 3 are 0.39 eV to 0.42 eV, 0.40 eV to 0.43 eV, and 0.41 eV to 0.44 eV, respectively. This finding indicates that dual PIT systems always maintain a large group index and good slow light effect. Furthermore, the transmission peak of the triple-PIT effect is tuned from 51% to 74%, and the group index of the triple-PIT system is controlled between 161.4 and 115.8 when the Fermi levels of graphene rectangle cavities 2 and 4 are 0.39 eV to 0.42 eV and 0.41 eV to 0.44 eV, respectively. Thus, the maximum group index is realized, and the best slow light effect can be obtained in the triple-PIT system. Meanwhile, as the intensity of the PIT transparent peak decreases at all PIT windows, the group index increases. The reason is that as the signal light takes more time to resonate in rectangle cavities, more light power is lost by scattering in the cavities. Therefore, the group index is enhanced at all PIT windows.

The resonant wavelengths of the three cavities are blue-shifted at the same time, the bandwidth is almost constant and the transmission spectrum changes more obviously with the increase of the Fermi levels of the three rectangle cavities, which is different from the bandwidth widening in the two cavities side-coupled with a graphene nanoribbon waveguide system. According to

$$n_{\mathrm{g}} = \frac{c}{l} \cdot \frac{\partial \theta(\omega)}{\partial \omega},$$

the group index increases. It is worth noting that the transmission phase shift in the triple PIT windows violently changes. In this ultracompact structure, the strong destructive interference near the transparent peak results in a more severe dispersion and a stronger coupling between the rectangle cavities. A mutation of the transmission phase shift can be obtained in this work. Hence, the stronger dispersion and coupling lead to the increase of the group index.

In addition, Han *et al.* proposed that the multiband PIT effect is dynamically tuned by a pump light.[26] The maximum transmission of the PIT effect is 58% when the intensity of the pump light is 5 MW·cm^{-2}, and the group index can reach 6. Dynamically tunable slow light effect is obtained using the pump light. However, a considerably large group index can be obtained, and an effective slow light effect can be achieved in the PIT system investigated in this study.

Table 4. Maximum transmission and group index of the dual- and triple-PIT systems under different Fermi levels of graphene rectangle cavities and pump light intensity at the peak wavelength of PIT.

Tuning method	System model	Corresponding parameters (eV)	Maximum transmission of PIT peak (%)	Maximum group index of PIT system
Graphene Fermi level	Dual-PIT effect of triple cavities side-coupled with waveguide system	$E_{\mathrm{F1}} = 0.39$, $E_{\mathrm{F2}} = 0.40$, $E_{\mathrm{F3}} = 0.41$	21	143.2
		$E_{\mathrm{F1}} = 0.40$, $E_{\mathrm{F2}} = 0.41$, $E_{\mathrm{F3}} = 0.42$	37	127.3
		$E_{\mathrm{F1}} = 0.41$, $E_{\mathrm{F2}} = 0.42$, $E_{\mathrm{F3}} = 0.43$	50	116.2
		$E_{\mathrm{F1}} = 0.42$, $E_{\mathrm{F2}} = 0.43$, $E_{\mathrm{F3}} = 0.44$	74	108.6
	Triple-PIT system	$E_{\mathrm{F1}} = 0.40$, $E_{\mathrm{F2}} = 0.39$, $E_{\mathrm{F3}} = 0.42$, $E_{\mathrm{F4}} = 0.41$	51	161.4
		$E_{\mathrm{F1}} = 0.40$, $E_{\mathrm{F2}} = 0.40$, $E_{\mathrm{F3}} = 0.42$, $E_{\mathrm{F4}} = 0.42$	62	144.8
		$E_{\mathrm{F1}} = 0.40$, $E_{\mathrm{F2}} = 0.41$, $E_{\mathrm{F3}} = 0.42$, $E_{\mathrm{F4}} = 0.43$	67	131.4
		$E_{\mathrm{F1}} = 0.40$, $E_{\mathrm{F2}} = 0.42$, $E_{\mathrm{F3}} = 0.42$, $E_{\mathrm{F4}} = 0.44$	74	115.8
Pump light intensity	Triple-PIT effect of four disk cavities side-coupled with a waveguide system	$I = 5$ MW·cm^{-2}	58[26]	6[26]

7. Conclusion

In summary, dynamic tunable multiband PIT effects are theoretically and numerically studied on the basis of considerable rectangle cavities coupled with a plasmon waveguide system by tuning the Fermi level of the graphene rectangle cavity. Two completely different realization methods are used to achieve single-PIT effect: one is the bright and dark mode coupling through direct destructive interference, and the other is the cavity coupled with a graphene nanoribbon waveguide through indirect destructive interference. In addition, dual-PIT effect is obtained by three rectangle cavities side-coupled with a graphene nanoribbon waveguide. The transmission of the dual-PIT effect can be significantly tuned between 0.21 and 0.74, and the corresponding group index is controlled between 143.2 and 108.6. This finding indicates that a large group index is maintained and a good slow light effect is realized in the dual-PIT system. Furthermore, the triple-PIT effect is achieved by combining bright–dark mode coupling and the cavities side-coupled with a graphene nanoribbon waveguide mechanism. The results reveal that considerably sharp trans-

parent windows of triple-PIT effect can be obtained, a high transmission is maintained between 0.51 and 0.74, and the corresponding group index is controlled between 161.4 and 115.8. Therefore, the maximum group index is realized, and the high transmission and the best slow light effect can be obtained in the triple-PIT system. The proposed structure is ultra-compact because its size is less than 0.5 μm^2 and considerably easier to fabricate than the proposed graphene-based metamaterial structures. Moreover, the slow light effect is more significant than the metal waveguide coupled structure. Therefore, the current study not only introduces a novel approach toward the realization of optical sensors and optical filters, but also has important application in slow light and light storage devices with ultrafast, ultracompact, multiband, and dynamic tunable.

Acknowledgments

Project supported by the National Natural Science Foundation of China (Grant Nos. 11647122 and 61705064), the Natural Science Foundation of Hubei Province, China (Grant Nos. 2018CFB672 and 2021CFB607), the Project of the Hubei Provincial Department of Education, China (Grant Nos. B2021215 and T201617), and the Natural Science Foundation of Xiaogan City, China (Grant Nos. XGKJ2021010002 and XGKJ2021010003).

References

[1] Yang X, Yu M, Kwong D L and Wong C W 2009 *Phys. Rev. Lett.* **102** 173902
[2] Harris S E 1997 *Phys. Today* **50** 36
[3] Hau L V, Harris S E, Dutton Z and Behroozi C H 1999 *Nature* **397** 594
[4] Liu J H, Yu Y F and Zhang Z M 2019 *Opt. Express* **27** 15382
[5] Longdell J J, Fraval E, Sellars M J and Manson N B 2005 *Phys. Rev. Lett.* **95** 063601
[6] Li H, Wang L, Liu J, Huang Z, Sun B and Zhai X 2013 *Appl. Phys. Lett.* **103** 211104
[7] Fan C Z, Jia Y L, Ren P W and Jia W 2021 *J. Phys. D: Appl. Phys.* **54** 035107
[8] Kekatpure R D, Barnard E S, Cai W and Brongersma M L 2010 *Phys. Rev. Lett.* **104** 243902
[9] Zhou L, Ye T and Chen J 2011 *Opt. Lett.* **36** 13
[10] Zhang X, Liu Z M, Zhang Z B, Gao E D, Luo X, Zhou F Q, Li H J and Yi Z 2020 *Opt. Express* **28** 36771
[11] Ge J H, You C L, Feng H, Li X M, Wang M, Dong L F, Veronis G and Yun M J 2020 *Opt. Express* **28** 31781
[12] Liu N, Langguth L, Weiss T, Kästel J, Fleischhauer M, Pfau T and Giessen H 2009 *Nat. Mater.* **8** 758
[13] Zhang S, Genov D A, Wang Y, Liu M and Zhang X 2008 *Phys. Rev. Lett.* **101** 047401
[14] Zhan S P, Kong D, Cao G T, He Z H, Wang Y, Xu G J and Li H J 2013 *Solid State Commun.* **174** 50
[15] Wang B Y, Zeng Q D, Xiao S Y, Xu C, Xiong L B, Lv H, Du J and Yu H Q 2017 *J. Phys. D: Appl. Phys.* **50** 455107
[16] Lai G, Liang R S, Zhang Y J, Bian Z Y, Yi L X, Zhan G Z and Zhao R T 2015 *Opt. Express* **23** 6554
[17] Zhang T, Zhou J Z, Dai J, Dai Y T, Han X, Li J Q, Yin F F, Zhou Y and Xu K 2018 *J. Phys. D: Appl. Phys.* **51** 055103
[18] Li H J, Wang L L and Zhai X 2016 *IEEE Photon. Technol. Lett.* **28** 1454
[19] He Z H, Ren X C, Bai S M, Li H J, Cao D M and Li G 2018 *Plasmonics* **13** 2255
[20] Zheng Z P, Luo Y, Yang H, Yi Z, Zhang J G, Song Q J, Yang W X, Liu C, Wu X W and Wu P H 2022 *Phys. Chem. Chem. Phys.* **24** 8846
[21] Zhang B H, Li H J, Xu H, Zhao M Z, Xiong C X, Liu C and Wu K 2019 *Opt. Express* **27** 3598
[22] Gao E D, Liu Z M, Li H J, Xu H, Zhang Z B, Luo X, Xiong C X, Liu C, Zhang B H and Zhou F Q 2019 *Opt. Express* **27** 13884
[23] Sun C, Si J N, Dong Z W and Deng X X 2016 *Opt. Express* **24** 11466
[24] Chai Z, Hu X, Yang H and Gong Q 2016 *Appl. Phys. Lett.* **108** 151104
[25] Zhan S, Li H, Cao G, He Z, Li B and Yang H 2014 *J. Phys. D: Appl. Phys.* **47** 205101
[26] Han X, Wang T, Li X M, Liu B, He Y and Tang J 2015 *J. Phys. D: Appl. Phys.* **48** 235102
[27] Zhu Y, Hu X, Fu Y, Yang H and Gong Q 2013 *Sci. Rep.* **3** 2338
[28] Han X, Wang T, Li X M, Liu B, He Y and Tang J 2015 *J. Lightwave Technol.* **33** 3083
[29] Celis A, Nair M, Taleb-Ibrahimi A, Conrad E, Berger C, Heer W and Tejeda A 2016 *J. Phys. D: Appl. Phys.* **49** 143001
[30] Lu H 2015 *Appl. Phys. B* **118** 61
[31] Wang L, Li W and Jiang X Y 2015 *Opt. Lett.* **40** 2325
[32] Noual A, Amrani M, Boudouti E H E, Pennec Y and Djafari-Rouhani D 2019 *Materials Today: Proceedings* **13** 1076
[33] Zhao H L, Ren Y, Fang L and Lin H 2020 *Results in Physics* **16** 102971
[34] Saraswat V, Jacobberger R M and Arnold M S 2021 *ACS Nano* **15** 3674
[35] Wang X R and Dai H J 2010 *Nat. Chem.* **2** 661
[36] Wang Q, Kitauta R, Suzuki S, Miyauchi Y, Matsuda K, Yamamoto Y, Arai S and Shinohara H 2016 *ACS Nano* **10** 1475
[37] Li F, Jackson S D, Grillet C, Magi E, Hudson D, Madden S J, Moghe Y, Brien C O, Read A, Duvall S G, Atanackovic P, Eggleton B J and Moss D J 2011 *Opt. Express* **19** 15212
[38] Xu H, Zhao M Z, Zheng M F, Xiong C X, Zhang B H, Peng Y Y and Li H J 2019 *J. Phys. D: Appl. Phys.* **52** 025104
[39] Xu H, Li H, He Z, Chen Z, Zheng M and Zhao M 2017 *Opt. Express* **25** 20780
[40] Wei B Z and Jian S S 2017 *J. Phys. D: Appl. Phys.* **50** 355101
[41] Wang T, Zhang Y, Hong Z and Han Z 2014 *Opt. Express* **22** 21529
[42] Lu H, Liu X M, Mao D, Gong Y K and Wang G X 2011 *Opt. Lett.* **36** 3233
[43] Lu H, Liu X M and Mao D 2012 *Phys. Rev. A* **85** 053803
[44] Ren T X and Chen L 2019 *Opt. Lett.* **44** 5446
[45] Neubert T J, Wehrhold M, Kaya N S and Balasubramanian K 2020 *Nanotechnology* **31** 405201
[46] Zhou F Q, Wang Y Q, Zhang X, Wang J W, Liu Z M, Luo X, Zhang Z B and Gao E D 2021 *J. Phys. D: Appl. Phys.* **54** 054002
[47] Zheng Z P, Zheng Y, Luo Y, Yi Z, Zhang J G, Liu Z M, Yang W X, Yu Y, Wu X W and Wu P H 2022 *Phys. Chem. Chem. Phys.* **24** 2527